



Article

Spatial Chirp of Agate Bands

Julia Goldbaum ¹, Charles Howard ²  and Avinoam Rabinovitch ^{3,*} 

¹ Physics Department, The Technological College of Beer Sheva, Beer Sheva 8410001, Israel; julia@post.bgu.ac.il

² Macabee Health Fund, Orthoped Department, Beer Sheva 8489312, Israel; Charles@inter.net.il

³ Physics Department, Ben Gurion University of the Negev, Beer Sheva 84105, Israel

* Correspondence: avinoam@bgu.ac.il; Tel.: +972-86461172

Received: 7 September 2019; Accepted: 12 October 2019; Published: 16 October 2019



Abstract: Agate bandwidths are analyzed and shown to consist of spatial chirps. It is shown that (a) bands are created by following an equal volume mode and (b) the spatial chirps are approximately spherical and concentrated at different “disturbance” locations in the individual agate sectors. Results indicate that the sequence of formation started with banding under a nonlinear process in a gel matrix and were secondarily deformed by external forces.

Keywords: agate bands; spatial chirp; chirp Fourier transforms

1. Introduction

Agates are beautiful and fascinating rocks found all around the world (see recent papers [1–4]). They are used as gems for their intricate colored patterns and as grinding materials for their hardness. Their diagenesis [5] remains enigmatic in spite of many studies over several decades.

The main feature of cut agates are the bands. These appear stacked one after the other, mostly—but not always—in parallel to the outside surface, and sometimes exhibiting different colors due, in part, to embedded impurities of diverse substances. In a previous publication [5] it was shown that these bands must develop during the sol–gel transition in geode genesis. However, their exact shape, especially their widths and how these widths change along the generation direction, have not been elucidated until now.

In this paper, we present our analysis of agate bandwidths and describe their inherent profile.

2. Materials and Methods

2.1. Materials

Slices of eight unpolished white-striped agate were obtained from Madagascar, along with three from Botswana and two from Australia. These agates were photographed in daylight with a Canon D5 Mark 2 full frame 21-megapixel camera. Then, 28 representative sequences of bands were chosen on these agates (Figure 1) and marked with a straight pencil line. The length of each sequence was measured with a ruler and stereomicroscope. The images were entered into FIJI image processing software [6] and converted to gray scale.

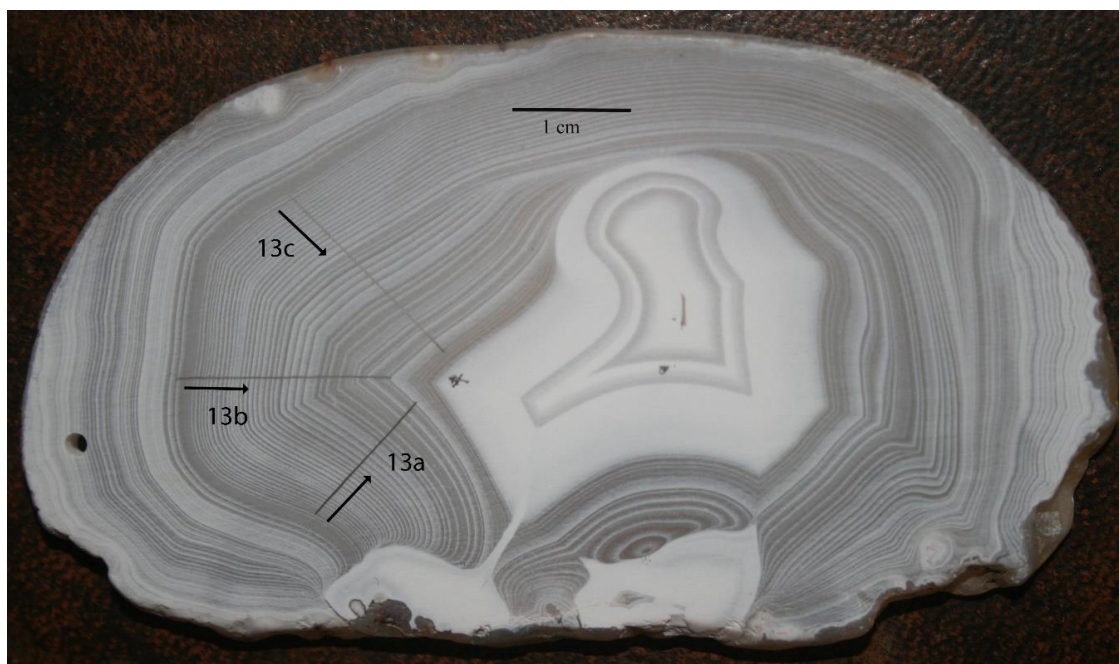


Figure 1. The cut section of a Madagascar agate. Three sequences of bands were chosen by drawing a pencil line (the thick black arrows show the direction these lines were analyzed).

The thin line is the line drawn as close to 90° to the bands as possible (hence not exactly parallel to the pencil line). The black graph above this line is the superimposed graph of the pixel values. As can be seen, it is also an accurate representation of the bands widths.

Using the “Line” tool, a grey line was added to the photograph and used to enable the software to set the scale of the picture. A second (thin line) was drawn as close to perpendicular to the bands as possible. Using the “Analyze” plug-in, a plot profile of the pixel values was made and exported to Excel. Thus, a measure of the variation of pixel values was obtained, which accurately mirrored the variations along the bands, including their widths (Figure 2). These pixel values were plotted against their distance, L , from the start of the line. The gradients of the graph were obtained by subtracting sequential “p” values, wherein gradient values of zero represented the minima and maxima of the graph. Thus, the distance between the maxima characterized the band widths.

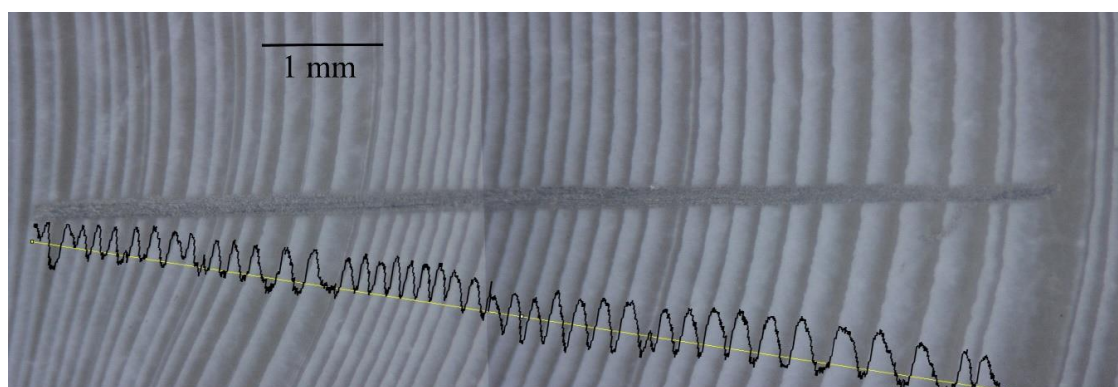


Figure 2. Representative sequence of bands from a Madagascar agate.

2.2. Analysis

In signal analysis, the “frequency” characterizes the number of bands per unit length and its inverse is the bandwidth.

Bandwidth is not constant throughout the agate, but rather changes with progress. These changes are not even. Moving from left to right (outside-inwards) in Figure 3, firstly, there are rapid changes with position, which probably correspond to sudden changes during the agate formation process. Following that, the change becomes continuous, i.e., the frequency decreases towards a “center” direction (Figure 3). This latter change type is observed in different samples. Details of these changes can give useful information relating to the formation of the agate (see discussion).

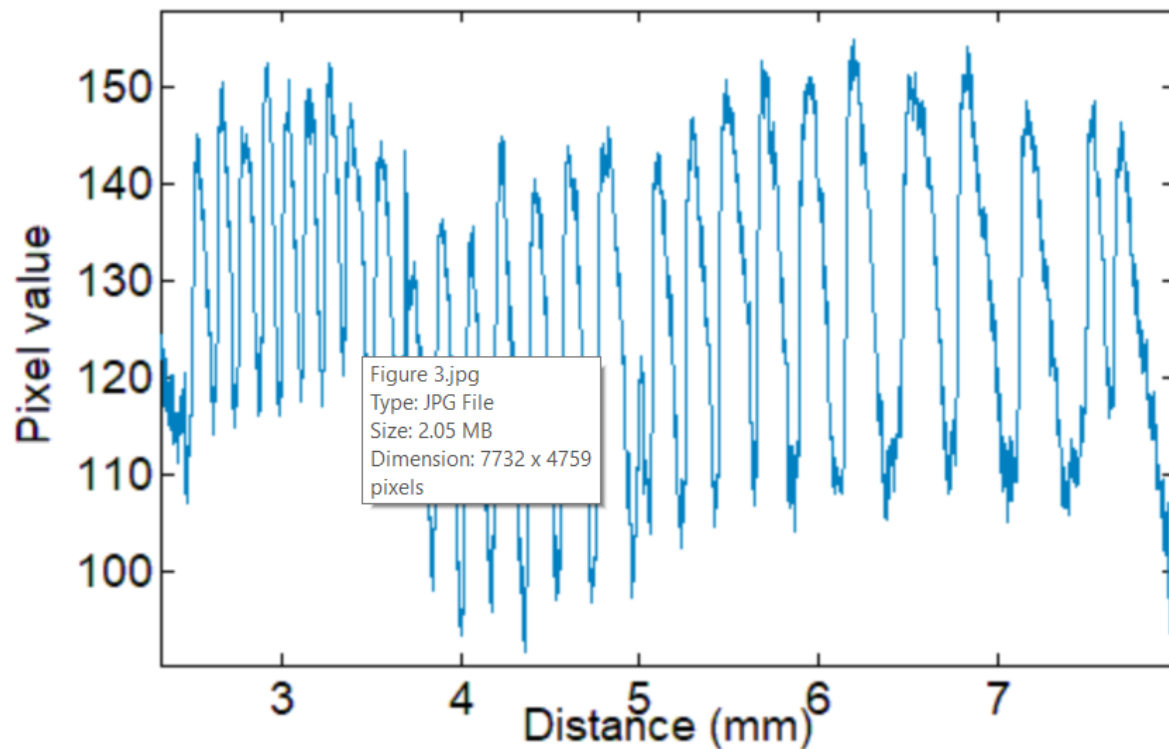


Figure 3. Changes of pixel values with position.

Signals of varying temporal frequency appear in radar measurements [7,8]. Such signals are called chirps and have been thoroughly studied in order to analyze signals obtained from moving targets [7]. The mathematical form of the signal's frequency variation can be different: linear, polynomial, exponential, etc. [7,8]. The Fourier frequency spectra for simple forms of the temporal frequency changes, e.g., a linear increase/decrease of frequency, are given in Reference [9].

A convenient method to obtain the spectrum is the fast Fourier transform (FFT). Here, it was carried out using MATLAB programming. In order to gain an understanding of these spectra, we measured surrogate temporal sinusoidal chirps. These chirps had a temporal frequency (TF) that changed with time between similar values to the spatial agate chirps (from 20 Hz to 16 Hz, a 20% decrease) in different ways: (a) linear, (b) quadratic, (c) 1.5 power and (d) square-root for pulses of short durations as encountered for our measurements (not shown). For chirp spectra and Fourier analysis, the reader is referred to the excellent article by Flandrin [10]. The spectral form is sensitive to the chirp type and duration.

Carrying out the agates' spatial frequency (SF) changes, similar shapes to the TF were obtained. In Figure 4a, an example of such spatial profiles is shown, taken from the data for Madagascar agate No. 12B. It looks very much like a saw-tooth pattern. Now, suppose that the color intensity changes sinusoidally in the form: $\sin[2\pi f_i(x_i + d)]$, which would be the first term in a Fourier series of the pattern. Note that the first term in the Fourier series of any repeating wave (including a saw-tooth), besides giving the best first approximation to the form, also provides the main frequency spectrum of it.

In Figure 4b, the Fourier transform for the profile shown in Figure 4a is depicted. Similarity with the second power change for quadratic chirp (b) is apparent.

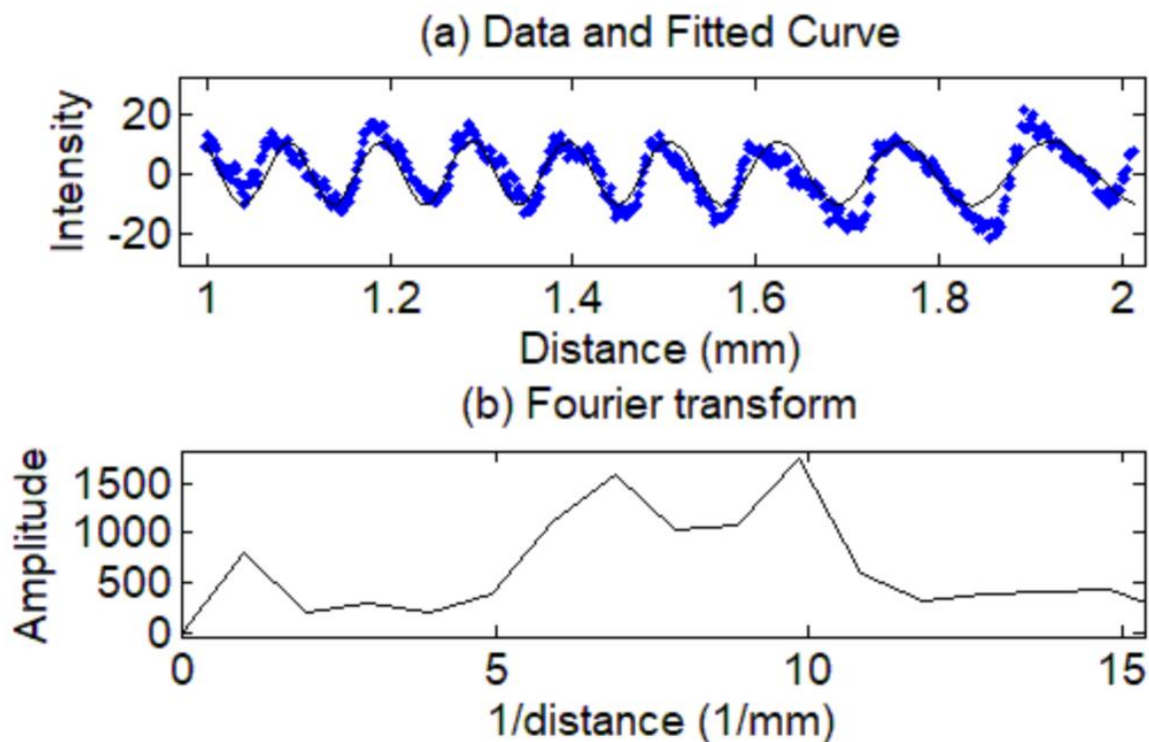


Figure 4. (a) Experimental data along with a sinusoidal fitting curve and (b) the Fourier transform, similar to a quadratic chirp, for Agate No. 12B (with a frequency decrease as the square root of distance).

In order to investigate the exact changes of the bands' widths, instead of using the whole "sinusoidal" shape, only maxima coordinates, x_i , were considered.

Although not proven, it would appear that agates are formed from a precursor sol/gel of silica [5,11–14]. We assumed that the bands developed in the globular shape manner by adding approximately spherical shaped layers of equal volume one on top of the other around different center locations within the agates. This assumption will be shown later (by an analysis of the measurements) to be valid.

The volume, V , of a spherical band of width b at a distance r from the sphere center is:

$$V = \left(\frac{4}{3}\right)\pi[(r+b)^3 - r^3] \quad (1)$$

According to Newton's binomial equation:

$$(r+b)^3 = r^3 + 3r^2b + 3rb^2 + b^3 \quad (2)$$

If $b \ll r$, then

$$(4/3)\pi(r+b)^3 \cong (4/3)\pi(r^3 + 3r^2b) \quad (3)$$

And: $V \cong 4\pi r^2 b$.

For equal bands volumes,

$$V_i = V(\text{const.}) = 4\pi r_i^2 b_i \quad (4)$$

Here, r_i is the average radius of the band (with respect to the specific center) and b_i is the widths of the bands along the radius (see Figure 5). Hence,

$$b_i = V/4\pi r_i^2 \quad (5)$$

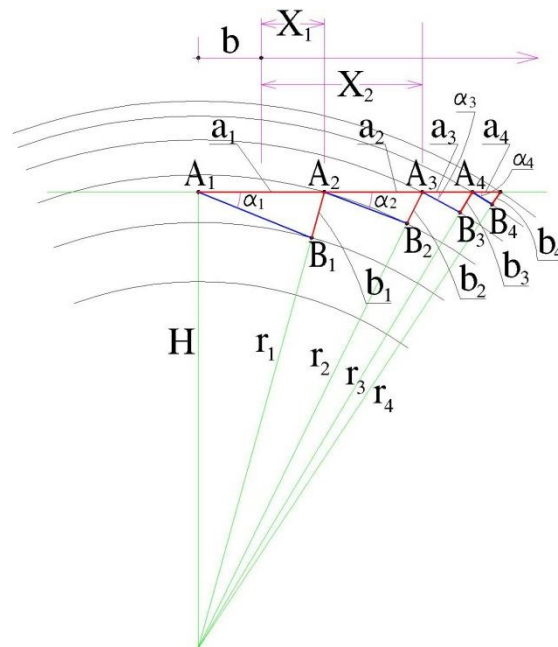


Figure 5. Cut surface geometry: r_i is the radius of the given point, H is the distance from the agate center to the cut surface, and x_i is the distance from the cut circle center to the given point along the cut surface.

However, we do not measure the b_i directly but only the “widths” a_i on the agate’s cut surfaces. For large r values:

1. The lines A_1B_1 , A_2B_2 etc. are approximately tangent to the circles. Hence:
2. The angles $A_1B_1A_2$ etc. are approximately 90° , and
3. The angles $B_1A_1A_2$ etc. i.e., α , α' etc. are approximately equal.

Therefore, to a first approximation,

$$a_i = \frac{b_i}{\sin \alpha} = V/4\pi r_i^2 \sin \alpha \quad (6)$$

Or:

$$f_i = \frac{1}{a_i} = 4\pi r_i^2 \sin \alpha / V \quad (7)$$

where f_i is the spatial frequency.

Again, we measure the “radii”, x_i , from a certain location on the cut surface. Therefore,

$$r_i^2 = H^2 + (d + x_i)^2 \quad (8)$$

where d can be either positive or negative, depending on the chosen center location (see Figure 5).

Or:

$$f_i \cong f_0 + C(d + x_i)^2 \quad (9)$$

where $C = 4\pi \sin \alpha / V$ and $f_0 = CH^2$, the initial frequency, C , f_0 , and d , are constants for a specific case.

As stated above, the results, shown in Figure 4, resemble a repeating saw-tooth pattern. Approximating them in the form, the wave maxima are therefore given by:

$$n_i = f_i(x_i + d) - \frac{1}{4} \quad (10)$$

Or:

$$n_i = [f_0 + C(x_i + d)^2](x_i + d) - 1/4 \quad (11)$$

3. Results

We fitted 28 measured samples to this frequency expression by a least square method. An example of a fitting to this relation is shown in Figure 6, with the obtained fitting parameters. The results of the fitting for different samples are given in Table 1. Importantly, an R-squared value for all the fitted samples is seen to be larger than 0.97.

Our fitting results gave values for the former f_0 between 1 mm^{-1} and 5.3 mm^{-1} (average and standard deviation were 2.66 mm^{-1} and 1.96 mm^{-1} , respectively).

Since f is the spatial frequency, $1/f$ is the layer thickness, which ranged between 0.19 mm and 1.00 mm, with an average and standard deviation of 0.44 mm and 0.41 mm, respectively.

The fitted values of the frequency change speed (C) were small, ranging between 0.001 mm^{-2} and 0.86 mm^{-2} , with an average and standard deviation of 0.076 mm^{-2} and 0.16 mm^{-2} , respectively. This shows that the changes in layer thickness are not drastic, but rather slow. The values of d , the initial points relative to the agate center from which we began to measure “radii”, ranged between 0.043 and 1.39 mm, with an average and standard deviation of 0.44 mm and 0.58 mm, respectively. This shows that the bands do not seem to be concentrated around the geometric centers of the agates, but rather around pseudo-centers, which can be points of disturbance (see below).

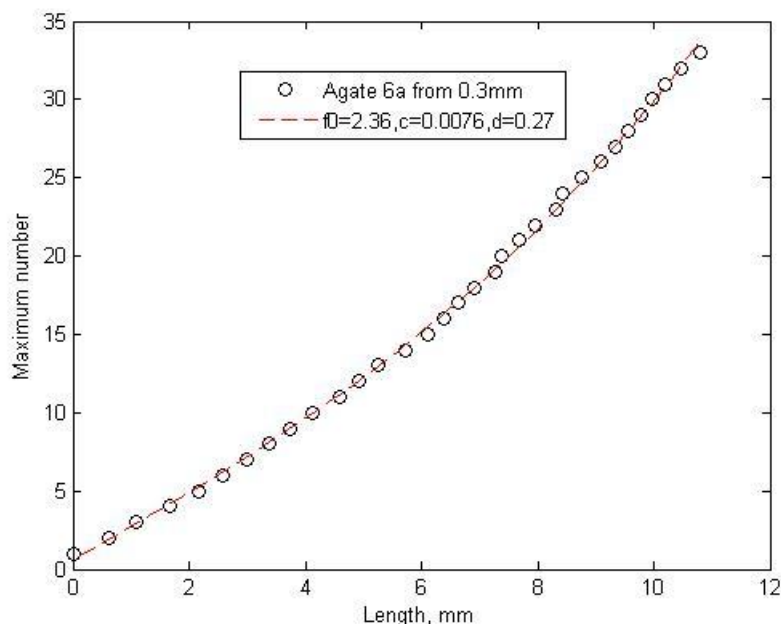


Figure 6. Example of a fitting result for Agate No. 6A.

4. Discussion

The measure of fit between a formula and a set of measured results is given by R^2 . The closer R^2 is to 1.0, the better the fit. In our case, the fit was excellent ($R^2 > 0.995$ for all agates), indicating the formulas were in exceptional agreement with the measurements. The closeness of R^2 to 1 thereby confirms the assumption of an equal volume hypothesis of the agate band formation. We studied

volcanic agate geodes from three different locations and the results were in agreement. Whether other forms (e.g., sedimentary, vein agates) follow the same rules is not possible to say and further analysis of these types of agate is necessary.

The appearance of agate bands is definitely due to a nonlinear reaction–diffusion–advection system, somewhat similar to the Belousov–Zhabotinsky (see, for example, References [15,16]) and Liesegang (see, for example, References [17,18]) phenomena. Since the exact materials participating in the reaction and the reaction and diffusion constants are unknown, a rigorous mathematical simulation is unattainable. Note that, in the Belousov–Zhabotinsky situation, equal volume bands appear in a test tube and, in the agate case, the chirp (equal volume bands) results from the spherical geometry involved.

The question arises of how the banding developed from both a temporal and spatial aspect. The data indicates (and see also Reference [5]) that the initiation process took place either from outside inwards or from inside progressing outwards at a single point in time and all the bands were formed fairly rapidly. Later, whilst still in the gel condition, external forces deformed the bands into the sectors seen in the agates, creating disturbance points. In a later period, this gel solidified, freezing the patterns in situ. After distortion of the gel spheres by secondary forces, the present state of the agate samples do not consist of whole perfect spherical bands; nevertheless, sufficient portions of these remain, allowing the equal volume assumption (as vindicated by the almost perfect correlation for all measurements, $R^2 > 0.995$, shown in Table 1).

Table 1. Fitting results.

Sample No.	Origin	Range	f_0 , Initial Frequency	C, Frequency Change Speed	d, mm ($\alpha = 2$)	Distance between Maxima, $1/f_0$	R^2
1C	Madagascar	From 1.5 mm to end	1.21	0.0066	1.004	0.82645	0.9924
1A	Madagascar	From 3 mm to end	2.02	0.0095	0.27	0.49505	0.9967
1A	Madagascar	All	1.86	0.0051	0.15	0.53763	0.9983
11B	Madagascar	To 3.5 mm	1	0.0824	0.85	1	0.9765
13B	Madagascar	All	2.52	0.0083	0.17	0.39683	0.9979
13B	Madagascar	From 1.3 mm to end	3	0.01	0.05	0.33333	0.997
15	Madagascar	All	2.39	0.001	0.1	0.41841	0.9963
6A	Madagascar	All	2.32	0.007	0.45	0.43103	0.9993
6A	Madagascar	From 0.3mm	2.36	0.0076	0.27	0.42373	0.9992
7A	Madagascar	All	1.81	0.0036	1.35	0.55249	0.9983
7A	Madagascar	From 1.5mm	1.94	0.005	0.5	0.51546	0.9983
12	Madagascar	All	3	0.0191	0.59	0.33333	0.9931
12A	Madagascar	From 1.25 to 7.4 mm	2.46	0.0437	0.6	0.4065	0.9939
12B	Madagascar	From 2.5 to 7 mm	2.82	0.0977	0.22	0.35461	0.9932
9	Madagascar	All	2.74	0.001	1.39	0.36496	0.9896
20	Botswana	All	4.8	0.14	0.05	0.20833	0.9991
20	Botswana	From 0.53 mm	5.14	0.179	0.126	0.19455	0.9987
21	Botswana	All	5.3	0.006	0.043	0.18868	0.9959
21	Botswana	From 3.7 mm	1.32	0.864	0.64	0.75758	0.9981
22	Botswana	From 3 to 6.5 mm	1.86	0.0477	0.43	0.53763	0.9921
22	Botswana	From 3 mm	2.56	0.0018	0.11	0.39063	0.9848
25	Australia	All	3.13	0.01	0.52	0.31949	0.9913
25	Australia	From 1.3 mm	2.54	0.027	0.64	0.3937	0.9922
25	Australia	From 1.9 mm	2.42	0.039	0.6	0.41322	0.9914
25	Australia	From 3.1 mm	2.19	0.091	0.47	0.45662	0.9892
26	Australia	All	2.83	0.08	0.28	0.35336	0.9971
26	Australia	From 0.28 mm	2.84	0.098	0.24	0.35211	0.9967
26	Australia	From 1.9 mm	3.98	0.227	0.188	0.25126	0.9988

5. Conclusions

The beauty of agates has been appreciated since Roman times for their colored banded structure. Perhaps one reason for this is an almost unconscious feeling that the bands have an order to them and are not simply a chaotic arrangement. However, analysis of this “order” and its mathematical description has remained elusive. In this work we have, for the first time, analyzed this structure and shown that, under a very simple assumption—that of a constant volume for each—the nature of the bands’ widths can be fully described. As Agates cannot be made in the laboratory, their mechanism of formation is unknown. Most previous hypotheses simply do not fit the observations or ignore them.

Thus, a working hypothesis of the distribution/width of the bands is an important factor in elucidation of the actual diagenesis of these special and exquisite rock formations.

In the future, we plan to use a reaction–diffusion–advection differential system to model band development both in agates and in our sol–gel experiments.

Author Contributions: Individual contributions to the article were as following: conceptualization, A.R. and C.H.; methodology, A.R. and C.H.; software, J.G., C.H.; formal analysis, J.G.; investigation, A.R., J.G.; writing—original draft preparation, J.G., C.H.; writing—review and editing, A.R., C.H.; visualization, J.G.; supervision and project administration, A.R.

Funding: This research received no external funding.

Conflicts of Interest: The authors declare no conflict of interest.

References

1. Götze, J.; Berek, H.; Schäfer, K. Micro-structural phenomena in agate/chalcedony: Spiral growth. *Mineral. Mag.* **2019**, *83*, 281–291. [[CrossRef](#)]
2. Richter-Feig, J.; Möckel, R.; Götze, J.; Heide, G. Investigation of fluids in macrocrystalline and microcrystalline quartz in agate using thermogravimetry-mass-spectrometry. *Minerals* **2018**, *8*, 72. [[CrossRef](#)]
3. Cidade, M.K.; Palombini, F.L.; Duarte, L.C.; Paciornik, S. Investigation of the thermal microstructural effects of CO₂ laser engraving on agate via X-ray microtomography. *Opt. Laser Technol.* **2018**, *104*, 56–64. [[CrossRef](#)]
4. Dumańska-Słowik, M.; Powolny, T.; Sikorska-Jaworowska, M.; Gaweł, A.; Kogut, L.; Poloński, K. Characteristics and origin of agates from Płóczki Górne (Lower Silesia, Poland): A combined microscopic, micro-Raman, and cathodoluminescence study. *Spectrochim Acta Part A: Mol. Biomol. Spectrosc.* **2018**, *192*, 6–15. [[CrossRef](#)] [[PubMed](#)]
5. Howard, C.B.; Rabinovitch, A. A new model of agate geode formation based on a combination of morphological features and silica sol–gel experiments. *Eur. J. Mineral.* **2018**, *30*, 97–106. [[CrossRef](#)]
6. Schindelin, J.; Arganda-Carreras, I.; Frise, E. Fiji: An open-source platform for biological-image analysis. *Nat. Methods* **2012**, *9*, 676–682. [[CrossRef](#)] [[PubMed](#)]
7. Djurović, I.; Simeunović, M.; Wang, P. Cubic phase function: A simple solution to polynomial phase signal analysis. *Signal Process.* **2017**, *135*, 48–66. [[CrossRef](#)]
8. Li, D.; Gui, X.; Liu, H.; Su, J.; Xiong, H. An ISAR imaging algorithm for maneuvering targets with low SNR based on parameter estimation of multicomponent quadratic FM signals and nonuniform FFT. *Appl. Earth Obs. Remote Sens.* **2016**, *9*, 5688–5702. [[CrossRef](#)]
9. Klauder, J.R.; Price, A.C.; Darlington, S.; Albersheim, W.J. The theory and design of chirp radars. *Bell Syst. Tech. J.* **1960**, *39*, 745–809. [[CrossRef](#)]
10. Flandrin, P. Time frequency and chirps. In Proceedings of the Wavelet Applications VIII, Orlando, FL, USA, 26 March 2001; International Society for Optical Photonics: Cardiff, Wales, 2001; Volume 4391, pp. 161–175. [[CrossRef](#)]
11. Wang, Y.; Merino, E. Self-organizational origin of agates: Banding, fiber twisting, composition, and dynamic crystallization model. *Geochim. Cosmochim. Acta* **1990**, *54*, 1627. [[CrossRef](#)]
12. Moxon, T.; Reed, S.J.B. Agate and chalcedony from igneous and sedimentary hosts aged from 13 to 3480 Ma: A cathodoluminescence study. *Mineral. Mag.* **2006**, *70*, 485–498. [[CrossRef](#)]
13. Möckel, R.; Götze, J.; Sergeev, S.A.; Kapitonov, I.N.; Adamskaya, E.V.; Goltsin, N.A.; Vennemann, T. Trace-element analysis by laser ablation inductively coupled plasma mass spectrometry (LA-ICP-MS). *J. Siberian Federal Univ. Eng. Technol.* **2009**, *2*, 123–138.
14. Zenz, J. *Agates III*; Bode Verlag: Lauenstein, Germany, 2011; p. 69.
15. Grzybowski, B.A.; Bishop, K.J.M.; Campbell, C.J.; Fialkowski, M.; Smoukov, S.K. Micro- and nanotechnology via reaction-diffusion. *Soft Matter* **2005**, *1*, 114–128. [[CrossRef](#)]
16. Mikhailov, A.S.; Showalter, K. Control of waves, patterns and turbulence in chemical systems. *Phys. Rep.* **2006**, *425*, 79–194. [[CrossRef](#)]

17. Hongwei, Z.; Enxiang, L.; Zhaohui, Z.; Xiaobin, D.; Yuxing, P. Smart polymers based on belousov-zhabotinsky reaction. *Prog. Chem.* **2011**, *23*, 2368–2376.
18. Kumar, D.K.; Steed, J.W. Supramolecular gel phase crystallization: Orthogonal self-assembly under non-equilibrium conditions. *Chem. Soc. Revs.* **2014**, *43*, 2080–2088. [[CrossRef](#)] [[PubMed](#)]



© 2019 by the authors. Licensee MDPI, Basel, Switzerland. This article is an open access article distributed under the terms and conditions of the Creative Commons Attribution (CC BY) license (<http://creativecommons.org/licenses/by/4.0/>).